Demonstration of Large Coupling-Induced Phase Delay in Silicon Directional Cross-Couplers

Wouter J. Westerveld, *Student Member, IEEE*, Jose Pozo, *Member, IEEE*, Suzanne M. Leinders, Mirvais Yousefi, *Member, IEEE*, and H. Paul Urbach

***Abstract*—We investigate directional couplers in silicon-on-insulator photonic technology. We theoretically and experimentally demonstrate a large coupling-induced phase delay that occurs when nearly all light is coupled from one waveguide to the other, i.e., when the coupler operates as a cross-coupler. We show that even a tiny asymmetry in the two waveguides of the coupler causes a significant additional phase delay. The observed change in the free-spectral-range of ring resonators from 5.0 nm to 6.4 nm is explained by a small 0.1% difference in the propagation constants of the two waveguides. Such a difference can be caused by for example a 1 nm difference in the widths of the two waveguides.**

***Index Terms*—Directional couplers, optical waveguides, integrated optics, optical devices, optical filters, silicon-on-insulator technology.**

I. Introduction

SILICON photonic micro-ring resonators have received large interest over the last decade ([1]–[3] provide reviews of this field). Usually, directional couplers are used to couple light to the resonators. They offer low loss and low reflections compared to alternatives such as multi-mode-interference couplers [4], [5]. Directional couplers consist of two parallel waveguides, separated by a very small gap such that light couples from one waveguide to the other. The coupling can be described using coupled mode theory [6]–[8]. Most often, two identical parallel waveguides are used. In a first approximation, the phase delay of propagation through the coupler can be approximated as the phase delay of an isolated waveguide. However, there has been recent interest in a more precise characterization of the couplers, and the correction on the propagation constant due to the vicinity of the second waveguide was numerically and experimentally studied in [9], [10]. These papers reported on a Mach-Zehnder interferometer with a ring coupled to one of its arms. It was shown that correcting the length of the other arm for the coupler-induced phase delay significantly improves the filter response. It has been numerically and theoretically demonstrated that coupler-induced phase delay has a deleterious effect on the response of higher-order filters based on a cascade of ring resonators, that is, for designs that did not take this effect into account [11]. We observed an additional phase delay that is particular to the regime when nearly all light couples from one waveguide to the other, i.e., in the cross-coupling regime. Directional couplers that operate in this regime may find their applications as low-loss waveguide crossings and in optical delay lines based on ring resonators [12], [13].

In this work, we measure the phase delay that is introduced by the directional coupler due to asymmetry in the waveguides. This additional phase delay vanishes for a coupler consisting of two identical waveguides, but we show that a tiny asymmetry in the waveguides causes a significant additional phase delay for the case that nearly all light couples from one waveguide to the other. In this regime, directional couplers operate as cross-couplers. We measure the directional coupler in a ring resonator, and observed a significant change in the free-spectral-range (FSR) of the resonator. The magnitude of the measured asymmetry between the two waveguides corresponds to a difference between the widths of the two waveguides as small as 1 nm, which is below the fabrication accuracy.

In the next section, we summarize coupled mode theory for directional couplers, universal theory of ring resonators, and their combination. This theory predicts an additional phase delay around the cross-coupling regime of slightly asymmetric directional couplers and a change in the FSR of ring resonators with such couplers. In Section III, we detail the studied devices and the characterization methodology. In Section IV, we find that the measured spectra show a large change in the free-spectra-range in the cross-coupling regime, agreeing very well with the theoretical relations. We conclude in Section V.

II. Theory

This section first describes relations for directional couplers employing coupled mode theory, and then presents the theory of ring resonators that are used to study the couplers.

Manuscript received October 1, 2013; revised November 22, 2013; accepted November 22, 2013. This work was supported by TNO and the IOP Photonic Devices program of NL Agency.

W. J. Westerveld is with the Optics Research Group, Faculty of Applied Sciences, Delft University of Technology, 2628CH Delft, The Netherlands and also with TNO, 2628CK Delft, The Netherlands (e-mail: w.j.westerveld@tudelft.nl).

J. Pozo is with the TNO, 2628CK Delft, The Netherlands (e-mail: jose.pozo@tno.nl).

S. M. Leinders is with the Laboratory of Acoustical Wavefield Imaging, Faculty of Applied Sciences, Delft University of Technology, 2628CH Delft, The Netherlands (e-mail: s.m.leindes@tudelft.nl).

M. Yousefi is with Photonic Sensing Solutions, 1013EN Amsterdam, The Netherlands (e-mail:m.yousefi@photonics2.com).

H. P. Urbach is with the Optics Research Group of the Faculty of Applied Sciences of Delft University of Technology, 2628CH Delft, The Netherlands (e-mail:h.p.urbach@tudelft.nl).

Color versions of one or more of the figures in this paper are available online at http://ieeexplore.ieee.org.

Digital Object Identifier 10.1109/JSTQE.2013.2292874

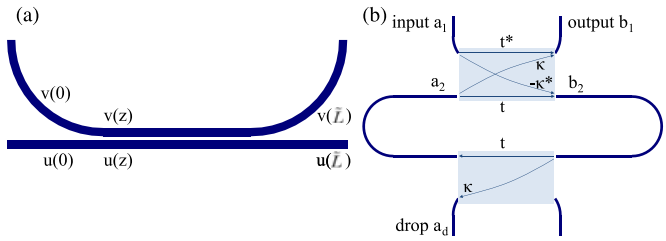

Fig. 1. (a) Sketch of a directional coupler, top-view. Waveguide width ∼400 nm, gap 220 nm. (b) Sketch of a racetrack-shaped ring resonator with two couplers (add-drop configuration), consisting of 400 nm wide waveguides. The straight track is 40 μm, and the bend radius is 5 μm. We used infrared light around free-space wavelength $\lambda_c = 1550$ nm.

A. Directional Couplers

The directional coupler consists of two close parallel single-mode waveguides so that power couples from one waveguide (labeled u) to the other [labeled v, see Fig. 1(a)]. Describing this system with perturbation theory, we assume that the electric field in the coupler can be approximated by a superposition of the two modes of the isolated waveguides [6]–[8]. The amplitudes of the two modes vary while propagating through the parallel waveguides due to the coupling (i.e., light "leaks" from one mode to another), as described by

$$\boldsymbol{E}(x,y,z,t) \approx \boldsymbol{\mathcal{E}}_u(x,y)u(z)e^{\imath\omega t} + \boldsymbol{\mathcal{E}}_v(x,y)v(z)e^{\imath\omega t}. \quad (1)$$

Let us consider the result of an excitation of mode u at $z = 0$ (i.e., all light is in waveguide u). The transmission of a coupler with length $\tilde{L}$ is given by $u(\tilde{L}) = tu(0)$, while the coupled light is given by $v(\tilde{L}) = \kappa u(0)$. These complex amplitudes t and κ can be calculated using coupled mode theory, see [6]–[8], giving

$$t = e^{-\imath(\beta_u + \kappa_{uu} - \delta)\tilde{L}} \left(\cos s\tilde{L} - \frac{\imath\delta}{s} \sin s\tilde{L} \right) \quad (2)$$

where β_u is the propagation constant of mode u, κ_{uu} is the correction to this propagation constant originating from the other waveguide, $\delta \equiv \frac{1}{2}(\beta_u + \kappa_{uu} - \beta_v - \kappa_{vv})$ is due to the difference between two waveguides, $s = \sqrt{\kappa_{uv}\kappa_{vu} + \delta^2}$ is the coupling coefficient dominated by κ_{uv} and κ_{vu}, and where we have used κ_{uv}, κ_{vu}, κ_{uu}, and κ_{vv} from [8]. Coefficients κ_{uv}, κ_{vu}, κ_{uu}, and κ_{vv} all depend on overlaps of the electric fields $\boldsymbol{\mathcal{E}}_u(x,y)$ and $\boldsymbol{\mathcal{E}}_v(x,y)$ in the cross-section of one of the two waveguides. Coefficient κ_{uu} scales with the intensity of the evanescent tail mode u that is the cross-section of waveguide v (the intensity of mode u scales with the overlap the electric field of this mode with itself). Coefficient κ_{uv} scales with the overlap of the electric fields of modes u and v that is in the cross-section of waveguide v. Coefficients κ_{vv} and κ_{vu} are similar to coefficients κ_{uu} and κ_{uv} but with u and v interchanged. The guides in the coupler we study are designed to be identical, but we observed non-zero δ in our couplers.

Equation (2) is valid for two parallel waveguides, whereas the actual coupler also includes bends to connect the parallel waveguides to the components in the circuit. We take the coupling which occurs in the bends into account by re-defining the length $\tilde{L}$ in (2) as an effective coupling length $\tilde{L} = L + \Delta L$, with L the length of the parallel waveguides.

The coupled mode formalism in [8] was derived for low index contrast waveguides, while silicon-on-insulator waveguides have a high refractive index contrast. Therefore, we compared coupled mode theory with the eigenmode expansion method and finite-difference-time-domain (FDTD) simulations. The coupling coefficients s as computed with the three different methods agree within 5% for couplers with two identical waveguides that have waveguide widths varying from 380 to 460 nm and gaps varying from 140 to 240 nm. In the eigenmode expansion, we computed s from the length L_π when most energy is transferred from waveguide u to waveguide v. This is when the phase difference between the symmetric (sm) and the anti-symmetric (am) modes of the configuration of the two parallel waveguides is π, giving $L_\pi = \pi/(\beta_{sm} - \beta_{am})$, and $s = (\beta_{sm} - \beta_{am})/2$. Throughout this work, modal profiles and propagation constants were computed using the film mode-matching (FMM) method as implemented in FimmWave (by Photon Design, Oxford, U.K.). In the FDTD simulations, we simulated a set of five directional couplers with L varying from 0 to 16 μm. In each simulation, we recorded the power transmission $|t_L|^2$ from the left-hand-side of the lower waveguide to the right-hand-side of the lower waveguide [see Fig. 1(a)]. Hereafter, we obtained the unknowns s and ΔL by fitting (2) for identical waveguides, i.e. $|t_L|^2 = \cos^2[s(L + \Delta L)]$, to the $|t_L|^2$ versus L plot.

Dispersion is taken into account by assuming linear dispersion of the effective index and linear dispersion of the coupling $s(\lambda) = s(\lambda_c) + s'(\lambda - \lambda_c)$. We neglected dispersion in ΔL, which is validated by the fact that the obtained relations accurately describe the measured spectra. The propagation constant $\beta(\lambda)$ can be expressed in the effective index n_e and effective group index $n_g \equiv n_e - \lambda \frac{\partial n_e}{\partial \lambda}$ evaluated at center wavelength $\lambda_c = 1550$ nm, giving

$$\beta(\lambda) = 2\pi \left[\frac{n_e - n_g}{\lambda_c} + \frac{n_g}{\lambda} \right]. \quad (3)$$

The phase shift due to traveling through the directional coupler is the argument of (2), i.e.,

$$\phi_t = -\beta_u \tilde{L} - (\kappa_{uu} - \delta)\tilde{L} + \arg\left\{ \cos s\tilde{L} - \frac{\imath\delta}{s} \sin s\tilde{L} \right\} \quad (4)$$

in which $\arg\{\}$ denotes the argument of a complex number. The first term is simply propagation through an isolated guide. The second term is small, and we could not observe it due to the fabrication uncertainty of β_u. The third term is usually small, apart from the cross-coupling regime where most light is coupled from one waveguide (u) to the other (v). The argument of a real number is zero, and the real part of the term inside the $\arg\{\}$ is usually much larger than the imaginary term as δ/s is small. However, the real part of this term vanishes around $\cos s\tilde{L} = 0$, hence this argument rapidly increases up to values of π rad. We observed this effect as a change in the FSR of the ring resonator.

B. Ring Resonators

The directional couplers were studied using ring resonators with circumference l. The optical power transmission T of a

micro-ring resonator with two lossless couplers in an add-drop configuration [Fig. 1(b)] is [14]

$$T = \frac{\alpha^2|t|^2 + |t|^2 - 2\alpha|t|^2\cos\theta}{1 + \alpha^2|t|^4 - 2\alpha|t|^2\cos\theta} \tag{5}$$

where $|t|^2$ is the straight-through power of the coupler, α is the transmission due to one round-trip ($\alpha = 1$ means zero loss). The phase delay of one round-trip through the ring $\theta = \phi_r + 2\phi_t$, with the phase delay due to propagation through the isolated waveguide of the ring $\phi_r = \beta_u(l - \tilde{L})$, and with ϕ_t the phase delay of the coupler. When a directional coupler is used to couple light to the ring, t and ϕ_t are given by (2) and (4), hence

$$\theta = -\beta_u l + 2\delta\tilde{L} + 2\arg\left\{\cos s\tilde{L} - \frac{\imath\delta}{s}\sin s\tilde{L}\right\} \tag{6}$$

in which the term $\kappa_{uu}\tilde{L}$ is neglected.

III. Characterization

We characterized integrated optical devices in silicon-on-insulator technology, having 220 nm thick rectangular waveguides of mono-crystalline silicon. The guides are on top of a 2 μm thick buried oxide (BOX) layer which is on top of a silicon substrate, and have a 2 μm thick SiO_2 cladding such that the silicon waveguides are embedded in silica. The devices were fabricated via the EU-funded ePIXfab consortium at IMEC (Leuven, Belgium) using their CMOS line with 193 nm deep-UV lithography [15], [16]. We measured the dimensions of the fabricated waveguides and couplers with a helium-ion-microscope (Carl Zeiss SMT), providing an accuracy of 15 nm. We have deposited the SiO_2 cladding using plasma-enhanced chemical vapor deposition (PECVD). We characterized a set of eleven directional couplers in racetrack-shaped ring-resonators (see Fig. 1), in which the length of the parallel waveguides L was varied from 0 to 18 μm.

We used an amplified spontaneous emission light-source (Opto-link ASE) to generate light around 1550 nm, coupled it to- and from the chip using on-chip out-of-plane grating couplers [17], [18], and recorded the transmission spectrum with an optical spectrum analyzer (Yokogawa AQ6370B OSA). The spectra were normalized to the transmission spectrum of a straight waveguide to correct for the grating coupler transmissions. In order to remove the Fabry-Pérot reflections in this reference spectrum, it was smoothened by a convolution with a Gaussian window with a full-width at half-max (FWHM) of 1 nm. Datapoints in the ring transmission spectrum below -80 dB/nm were clipped because this is the noise floor of the OSA.

Equation (5) with (6) and (3) was fitted to the recorded spectra. The parameters that are fitted are: coupling coefficient s, dispersion in the coupler $s' \equiv \partial s/\partial\lambda$, asymmetry in the coupler δ, the effective index n_e with linear wavelength dependency (described by n_g), and a wavelength-independent correction for coupling in the bends ΔL. We have independently measured the wavelength-dependent losses of straight and bend waveguides to calculate the ring round-trip loss (or transmittance $\alpha(\lambda)$). In a spectrum between 1535 nm and 1565 nm, the average loss of the straight waveguide was -2.5 dB/cm, and the average loss of a 180° bend with 5 μm radius was -0.024 dB. The spectra of the set of resonators with a varying length of the coupler L are used simultaneously in the fitting. Single values for s, s', ΔL, δ, and n_g are fitted. The resonance wavelengths depend strongly on the effective index, which varies from device to device due to fabrication. This can be seen in the upper three plots of Fig. 2, in which the resonances are not exactly at the same wavelength. Therefore device-specific effective indices are fitted ($\{n_e\}$, with the curly brackets indicating that this is a set of numbers). The input power, $\{P_0\}$, is also fitted from measurement-to-measurement, as it depends on the alignment of the optical fibers with respect to the chip.

The equations are fitted to the spectra by minimizing least-square difference between the computed transmission, $T(\lambda)$, and the measured spectra. Each datapoint (wavelength) in this minimization is weighted with $1/I$, with I the average measured transmission in a 5 nm wavelength span around this wavelength. This 5 nm corresponds to approximately one FSR. The fitting is done in the intensity domain (not in the logarithmic dB scale) thus without weighting, the noise (or spurious reflections) in the $L = 0$ μm spectrum would have more influence than the signal in the $L = 14$ μm spectrum. The Matlab implementation of the Levenberg-Marquardt optimization is used for the fitting [19].

An accurate initial estimate is required as starting point for the fitting to converge properly. The properties of the coupler s, ΔL, and n_g are estimated from a different analysis without coupler dispersion and asymmetry (see Appendix). This less complete method gave an accurate estimate, close to the values obtained using the full analysis. An accurate initial estimate of the resonance wavelengths is required. Therefore, these wavelengths were first found using the *findpeaks* algorithm [20]. Similar to the approach in the Appendix, the effective index as computed by the mode-solver is used to estimate the mode numbers m of the dips in the spectrum. Then for each resonance in the recorded spectrum, the effective index is calculated, and the mean effective index over all 5 or 6 resonances is used as initial estimate of n_e. As initial estimate, we chose $s' = 0$ μm^{-2} and $\delta = 0.002$ μm^{-1} (this gave best convergence). This procedure provided an initial estimate that is accurate enough for the fitting to converge.

IV. Results

Fig. 2 shows that the fitted spectra agree very well with the measured spectra, indicating that (5) and (6) indeed contain all important physical effects. We obtain $s = 0.10$ μm^{-1}, $\Delta L = 2.1$ μm, $\partial s/\partial\lambda = 0.41$ μm^{-2}, $\delta = 0.0042$ μm^{-1} and $n_g = 4.3$.

Length $L = 14$ μm is of special interest as it includes the cross-coupling regime and the corresponding change in the FSR is clearly visible. Equations (5) and (6) predict this change in the FSR of the ring due to the particular phase shift of the directional coupler around the situation where most light is coupled to the resonator (that is, when $|t|^2$ is minimal and $\cos[s(\lambda)\tilde{L}] = 0$). In one spectrum, $\tilde{L}$ is fixed but s varies slightly due to linear

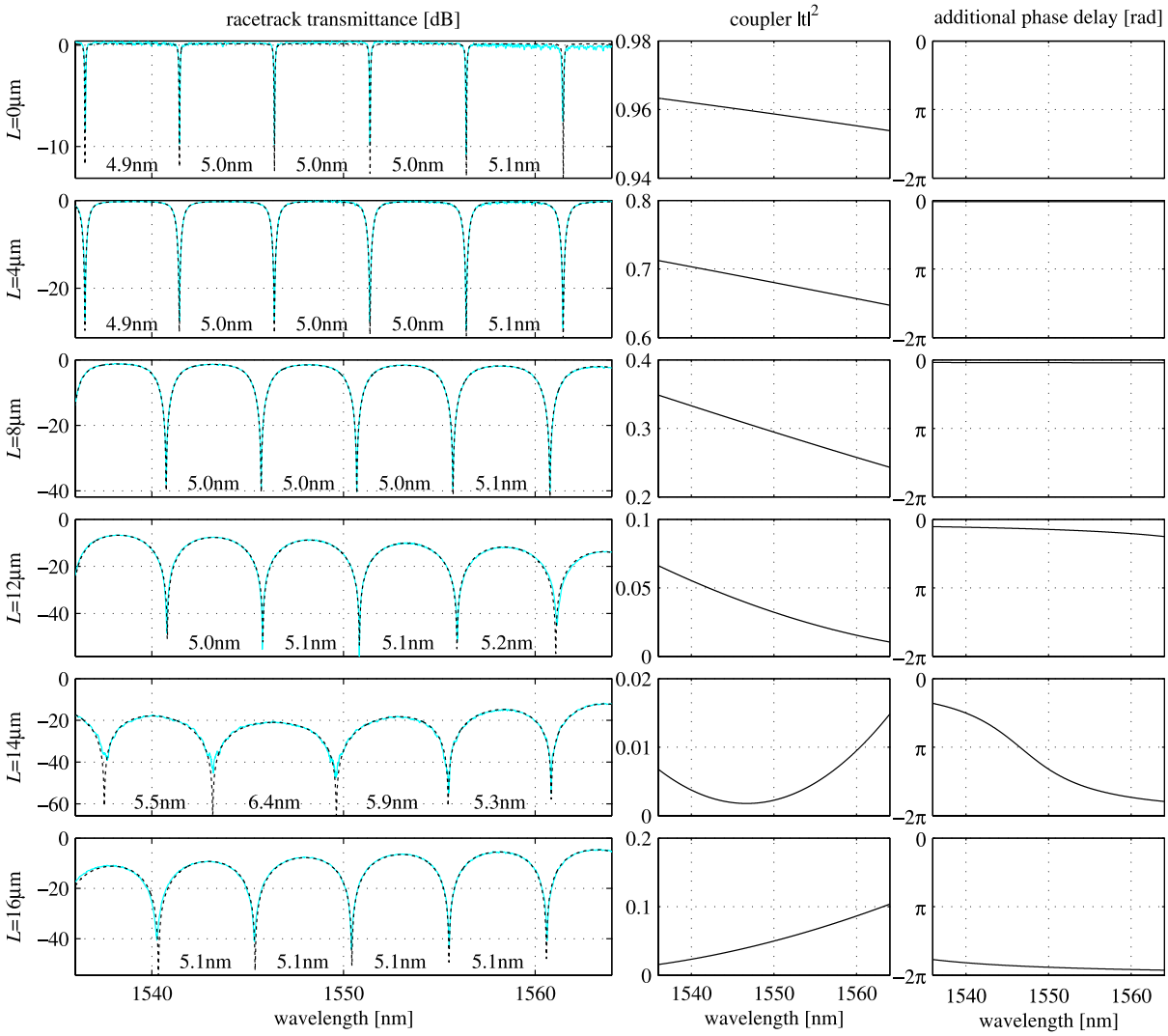

Fig. 2. Characterization of a set of racetrack resonators with two identical couplers. Waveguide width 394 nm and gap 168 nm. Each row shows a different length L of the parallel waveguides. Lengths 1 μm, 2 μm, 6 μm, 10 μm, and 18 μm are also taken into account in the analysis and fitting but not plotted here. Left column: measured transmittance spectrum (solid cyan lines) and fitted transmission function (dashed black lines). Middle column: Fitted value of the straight-through power in the coupler, $|t(\lambda)|^2$. Right column: Fitted value of the additional coupling-induced phase shift due to asymmetry, $2\arg\left\{\cos s\tilde{L} - \frac{\imath\delta}{s}\sin s\tilde{L}\right\}$.

dispersion $\partial s/\partial\lambda$. The straight-through power of the coupler, $|t|^2$, obtained from the fitting is shown in the middle column of Fig. 2 (note the y-axis) and the additional phase delay related to the asymmetry in the coupler is shown in the right column. For the $L = 14$ μm spectrum, maximal coupling $|t|^2 \approx 0$ occurs at a wavelength of 1547 nm. The corresponding change in FSR from 5.0 nm to 6.4 nm is visible in the measured spectrum. This significant change is explained by a small difference between the propagation constants in the guides, $2\delta/\beta$, of 0.1% (β is computed with the numerical mode solver).

To get a feeling for δ, we compute the difference in the widths of the waveguides that would give such an asymmetry. The corresponding difference in between the widths of the waveguides would be $\Delta w \approx \partial w/\partial\beta \cdot 2\delta = 1$ nm ($\partial w/\partial\beta$ was calculated using the FMM numerical mode solver and verified with an analytical approximate mode-solver [21]). This 1 nm difference is below the fabrication accuracy of the waveguides. Another explanation to the origin of δ lays in the asymmetry in the connecting waveguides of the coupler, as the upper waveguides are bent whereas the lower waveguides are straight.

The coupling coefficient obtained from fitting the transmission spectra is much lower than the one we obtained with numerical FDTD simulations ($s = 0.151$ μm^{-1}). This could be caused by imperfect PECVD deposition of the silicon-dioxide cladding, leaving low quality SiO_2 between the parallel waveguides of the coupler. We expect that this is unrelated to the observed large phase delay. This is because this particular phase delay was only observed in the cross-coupling regime ($|t|^2 \approx 0$) and shows a very strong wavelength-dependent or transmission-dependent behavior. A different cladding would not introduce such a strong wavelength dependent or transmission dependent effect. Moreover, all eleven measured spectra are simultaneously well described by (5) with (6) using the same values of s, s', δ, ΔL, and n_g, validating the theory. Therefore the asymmetry in the waveguides is the most likely explanation of this particular phase delay.

V. Conclusions

Even a tiny (nanoscale) asymmetry in the two waveguides of a directional coupler causes a significant additional phase delay in the particular cross-coupling regime where most light is coupled from one waveguide to the other. In silicon-on-insulator ridge waveguides, such asymmetries are practically inevitable due to nanometer-scale variations in the fabrication process.

We observed a change in the FSR of a ring resonator from 5.0 nm to 6.4 nm due to a small asymmetry in the waveguides of the coupler. The magnitude of this asymmetry corresponds to a 1 nm difference in the widths of the two waveguides.

Appendix
Alternative description neglecting asymmetries and dispersion in the coupler

An accurate initial estimate is necessary for the fitting as described in Section III to converge. Therefore, s, ΔL, and n_g are first estimated using an incomplete analysis described in this Appendix.

Neglecting asymmetries and dispersion in the coupler, Equation (6) describing the phase delay of one round-trip through ring reduces to $\theta = -\beta l$, or using (3),

$$\theta = -2\pi \left[\frac{n_e - n_g}{\lambda_c} + \frac{n_g}{\lambda} \right] l. \tag{7}$$

Equation (5) with (7) describes the transmission spectrum of a ring resonator. We independently measured α (wavelength-averaged, see Section III), we know the circumference of the racetrack l, leaving $|t|^2$, n_e, n_g as unknowns.

As throughout this work, n_e and n_g without explicit λ dependence are evaluated at λ_c, where $n_g \equiv n_e - \lambda \frac{\partial n_e}{\partial \lambda}$, thus $n_e(\lambda) = n_e + (n_e - n_g)(\lambda/\lambda_c - 1)$.

We recorded a set of transmission spectra of the racetrack resonators with different coupler lengths L (see the measured spectra in Fig. 2, solid cyan lines in the left column). In this analysis, we first fitted (5) with (7) to each recorded spectrum. Although the measured spectra are normalized to a reference spectrum, it was necessary to include the power inserted in the device, P_0, in the fitting, to correct for the fiber-chip alignment. The fitted unknowns are thus $|t_L|^2$, n_e, n_g and P_0. An accurate initial estimate of n_e and n_g (defining the resonance wavelengths λ_m) is necessary as starting point for the Levenberg-Marquardt fitting algorithm [19]. Therefore, the resonance wavelengths in the spectrum were first estimated using *findpeaks* [20]. The group index n_g was estimated from the average FSR between the resonances, using $n_g = \lambda_c^2/(\mathrm{FSR} \cdot l)$. The mode number m is estimated from the resonance equation, $m \approx n_e l/\lambda_c$, where the effective index n_e was calculated using the mode solver. The effective index n_e is then updated to match the resonance wavelength λ_m closest to λ_c (taking dispersion in $n_e(\lambda)$ into account using the estimated n_g). The fitting of (5) with (7) to the measured spectra was done in two iteration, first fitting $|t_L|^2$ and P_0, and then fitting all unknowns.

Having obtained $|t_L|^2$ for different lengths of the coupler L allows finding the unknown properties s and ΔL of the coupler. Neglecting asymmetries ($\delta = 0$), Equation (2) reduces to $|t_L|^2 = \cos^2[s(L + \Delta L)]$, which we fitted to the $|t_L|^2$ versus L curve. From this analysis, we obtained $s = 0.10\ \mu\mathrm{m}^{-1}$, $\Delta L = 2.0\ \mu$m, and $n_g = 4.2$ (we used the fitted n_g of the $L = 0\ \mu$m spectrum).

It is interesting to compare this analysis with the complete analysis of Section III; we use the left column of Fig. 2 to describe the differences. For the weak coupling, lengths $L = 0\ \mu$m and $L = 4\ \mu$m, the obtained transmission spectra are indistinguishable from the depicted results of the complete analysis. However, the measured spectrum with $L = 14\ \mu$m is not well described by the theory in this Appendix, as the FSR and the transmittance in between the resonances are wavelength-dependent. In that case, it is clearly necessary to include the dispersion and asymmetry of the coupler in the description.

Acknowledgment

The authors would like to acknowledge the EU-funded ePIXfab consortium for the fabrication of the photonic devices, with special thanks to Dr. P. Dumon and Dr. A. Khanna of IMEC (Leuven, Belgium) for the technical support. At TNO (Delft, The Netherlands), the authors would like to thank J. H. van den Berg for post-processing the chips, Dr. E. van Veldhoven for the helium ion microscope (HIM) images, and Dr. P. J. Harmsma and R. A. Nieuwland for the support in the photonics lab.

References

[1] W. Bogaerts, P. De Heyn, T. Van Vaerenbergh, K. De Vos, S. Kumar Selvaraja, T. Claes, P. Dumon, P. Bienstman, D. Van Thourhout, and R. Baets, "Silicon microring resonators," *Laser Photon. Rev.*, vol. 6, no. 1, pp. 47–73, 2012.

[2] S. Feng, T. Lei, H. Chen, H. Cai, X. Luo, and A. Poon, "Silicon photonics: From a microresonator perspective," *Laser Photon. Rev.*, vol. 6, no. 2, pp. 145–177, 2012.

[3] F. Morichetti, C. Ferrari, A. Canciamilla, and A. Melloni, "The first decade of coupled resonator optical waveguides: Bringing slow light to applications," *Laser Photon. Rev.*, vol. 6, no. 1, pp. 74–96, 2012.

[4] L. B. Soldano and E. C. M. Pennings, "Optical multi-mode interference devices based on self-imaging: Principles and applications," *J. Lightw. Technol.*, vol. 13, no. 4, pp. 615–627, 1995.

[5] D. J. Thomson, Y. Hu, G. T. Reed, and J.-M. Fedeli, "Low loss MMI couplers for high performance MZI modulators," *IEEE Photon. Technol. Lett.*, vol. 22, no. 20, pp. 1485–1487, Oct. 2010.

[6] A. Yariv and P. Yeh, *Photonics: Optical Electronics in Modern Communications*, ser. The Oxford Series in Electrical and Computer Engineering Series. Oxford, U.K.: Oxford Univ. Press, 2007.

[7] A. Hardy and W. Streifer, "Coupled mode theory of parallel waveguides," *J. Lightw. Technol.*, vol. 3, no. 5, pp. 1135–1146, Oct. 1985.

[8] A. Hardy, "A unified approach to coupled-mode phenomena," *IEEE J. Quantum Electron.*, vol. 34, no. 7, pp. 1109–1116, Jul. 1998.

[9] S. Darmawan, L. Y. M. Tobing, and T. Mei, "Coupling-induced phase shift in a microring-coupled Mach-Zehnder interferometer," *Opt. Lett.*, vol. 35, no. 2, pp. 238–240, Jan. 2010.

[10] L. Y. M. Tobing, L. Tjahjana, S. Darmawan, and D. H. Zhang, "Numerical and experimental studies of coupling-induced phase shift in resonator and interferometric integrated optics devices," *Opt. Express*, vol. 20, no. 5, pp. 5789–5801, Feb. 2012.

[11] M. Popovic, C. Manolatou, and M. Watts, "Coupling-induced resonance frequency shifts in coupled dielectric multi-cavity filters," *Opt. Express*, vol. 14, no. 3, pp. 1208–1222, Feb. 2006.

[12] A. Meijerink, C. G. H. Roeloffzen, R. Meijerink, L. Zhuang, D. A. I. Marpaung, M. J. Bentum, M. Burla, J. Verpoorte, P. Jorna, A. Hulzinga, and W. van Etten, "Novel ring resonator-based integrated photonic beamformer for broadband phased array receive antennas—Part I: Design and performance analysis," *J. Lightw. Technol.*, vol. 28, no. 1, pp. 3–18, 2010.

[13] L. Zhuang, M. Hoekman, W. Beeker, A. Leinse, R. Heideman, P. van Dijk, and C. Roeloffzen, "Novel low-loss waveguide delay lines using vernier ring resonators for on-chip multi-λ microwave photonic signal processors," *Laser Photon. Rev.*, vol. 7, no. 6, pp. 994–1002, 2013.
[14] A. Yariv, "Universal relations for coupling of optical power between microresonators and dielectric waveguides," *Electron. Lett.*, vol. 36, no. 4, pp. 321–322, 2000.
[15] P. Dumon, W. Bogaerts, A. Tchelnokov, J.-M. Fedeli, and R. Baets, "Silicon nanophotonics," *Future Fab Int.*, vol. 25, pp. 29–36, Apr. 2008.
[16] J. Pozo, P. Kumar, D. M. R. Lo Cascio, A. Khanna, P. Dumon, D. Delbeke, R. Baets, M. Fournier, J. Fedeli, L. Fulbert, L. Zimmermann, B. Tillack, H. Tian, T. Aalto, P. O"Brien, D. Deptuck, J. Xu, X. Zhang, and D. Gale, "Essential: Epixfab services specifically targeting (sme) industrial takeup of advanced silicon photonics," in *Proc.14th Int. Conf. Transparent Opt. Netw.*, 2012, pp. 1–3.
[17] D. Taillaert, F. van Laere, M. Ayre, W. Bogaerts, D. van Thourhout, P. Bienstman, and R. Baets, "Grating couplers for coupling between optical fibers and nanophotonic waveguides," *Jpn. J. Appl. Phys.*, vol. 45, no. 8A, pp. 6071–6077, Aug. 2006.
[18] W. J. Westerveld, H. P. Urbach, and M. Yousefi, "Optimized 3-d simulation method for modeling out-of-plane radiation in silicon photonic integrated circuits," *IEEE J. Quantum Electron.*, vol. 47, no. 5, pp. 561–568, May 2011.
[19] J. J. Moré, "The levenberg-marquardt algorithm: Implementation and theory," in *Numerical Analysis*, vol. 630, ser. Lecture Notes in Mathematics, G. Watson, Ed. Berlin/Heidelberg, Germany: Springer-Verlag, 1978, pp. 105–116.
[20] T. O'Haver. (2012, 9) Findpeaks matlab function by Tom O'Haver, [Online]. Available: http://terpconnect.umd.edu/˜toh/
[21] W. J. Westerveld, S. M. Leinders, K. W. A. van Dongen, H. P. Urbach, and M. Yousefi, "Extension of marcatili's analytical approach for rectangular silicon optical waveguides," *J. Lightw. Technol.*, vol. 30, no. 14, pp. 2388–2401, 2012.

Wouter J. Westerveld (M'10) received the M.Sc. degree in applied physics (*cum laude*) in 2009 from the Delft University of Technology, Delft, The Netherlands, where he is currently working toward the Ph.D. degree, in collaboration with TNO.

He is interested in applied physics in general and in silicon integrated micro optomechanical systems in particular.

Mr. Westerveld was a Board Member of the Student Association for Applied Physics (VvTP) at Delft University in 2004–2005. He was a Secretary (2011) and Chairman (2012) of the Student Board of the IEEE Photonics Society Benelux Chapter. He is a Certified Project Management Associate (IPMA Level D).

Jose Pozo graduated from the Universidad Publica de Navarra, Madrid, Spain, and Vrije Universiteit Brussel, Brussels, Belgium, as an Electrical Engineer with the M.Sc. degree in telecommunications in 2002, and the Ph.D. degree in 2006 from the University of Bristol, Bristol, U.K. on dilute nitride lasers for broadband communications.

In 2007, he joined the COBRA Research Institute, Eindhoven, The Netherlands, where he was a Postdoctoral Researcher on the study of chaotic semiconductor lasers as emitter and receivers of a chaos-encrypted communication link; and on the development of a novel concept for an integrated tunable laser based on filtered feedback. In 2010, he joined TNO as a EU Proposal Coordinator and a Scientist Specialist in integrated optics.

Since 2012, Dr. Pozo has been a member of the board of IEEE Benelux Photonics Society.

Suzanne M. Leinders received the M.Sc. degree in applied physics from the Delft University of Technology, Delft, The Netherlands, in 2010, where she is currently working toward the Ph.D. degree.

Her research interest includes medical acoustical imaging.

Mirvais Yousefi (M'99) received the M.Sc. degree in physics from the University of Lund, Lund, Sweden in 1998. He continued toward the Ph.D. degree at the Vrije Universiteit Amsterdam, Amsterdam, The Netherlands, in 2003.

Since then he has been a Postdoc at the Vrije Universiteit Amsterdam, the Vrije Universiteit Brussel, Brussel, The Netherlands, and the COBRA institute in Eindhoven, and as a Top Technologist at TNO in Delft, switzerland. Currently, he owns Photonic Sensing Solutions in Amsterdam. His major research interests are in laser dynamics and commercial photonic sensing technology.

Dr. Yousefi is the chairman of the IEEE Benelux Photonics Society.

H. Paul Urbach graduated in 1981 from the University of Groningen in The Netherlands, where he received the Ph.D. thesis in 1986 on the optimization of hydrodynamic propulsion.

He joined Philips Research Laboratory in Eindhoven, The Netherlands, in 1986. In 1994, he became a Principal Scientist at Philips Research Laboratory. In 2000, he became a Part-time Professor in diffraction optics at the Delft University of Technology, Delft. The Netherlands. Since January 2008, he has been a Full Professor and the Head of the Optics Research Group of the same university.

Dr. Urbach is the President-elect of the European Optical Society.